
Graph Random Features for Scalable Gaussian Processes

Matthew Zhang¹ Jihao Andreas Lin^{1,2} Adrian Weller^{1,3} Richard E. Turner^{1,3}
Isaac Reid¹

¹University of Cambridge

²Max Planck Institute for Intelligent Systems ³Alan Turing Institute

matthew.zhang473@gmail.com ir337@cam.ac.uk

Abstract

We study the application of *graph random features* (GRFs) – a recently-introduced stochastic estimator of graph node kernels – to scalable Gaussian processes on discrete input spaces. We prove that (under mild assumptions) Bayesian inference with GRFs enjoys $\mathcal{O}(N^{3/2})$ time complexity with respect to the number of nodes N , compared to $\mathcal{O}(N^3)$ for exact kernels. Substantial wall-clock speedups and memory savings unlock Bayesian optimisation on graphs with over 1M nodes on a single computer chip, whilst preserving competitive performance.

1 Introduction and related work

Gaussian processes (GPs) provide a powerful framework for learning unknown functions in the presence of uncertainty [1]. In certain applications, kernels based on Euclidean distance may be unsuitable – e.g. when modelling traffic congestion, since pairs of locations that are spatially close may not be connected by roads. In this case, kernels defined on the nodes of a graph \mathcal{G} may be more appropriate [2], [3]. One can then perform inference and make principled predictions, including during Bayesian optimisation, using GPs on graphs.¹

Scalability of GPs on graphs. Like their Euclidean cousins, exact GPs on graphs incur $\mathcal{O}(N^3)$ time complexity with respect to the number of nodes N . This makes them impractical when working with very large graphs. To mitigate this, practitioners use techniques such as ‘graph Fourier features’, which approximate the kernel matrix with a truncated eigenvalue expansion, or specific kernel families known to be sparse [3]. The former loses high-frequency kernel information and the latter limits flexibility. Alternatively, one can use kernels for small, local subgraphs, at the cost of no longer performing inference on the whole of \mathcal{G} [5].

Graph random features. In this paper, we propose to instead use the recently-introduced class of *graph random features* (GRFs) – sparse, unbiased estimates of graph node kernels computed using random walks [6], [7]. GRFs are Monte Carlo estimators of power series of weighted adjacency matrices, analogous to Von Neumann’s celebrated Russian Roulette estimator [8], [9]. GRFs enjoy strong concentration properties [10]. They are able to estimate a flexible class of graph node kernels – including the popular diffusion and Matérn kernels – by varying the so-called ‘modulation function’.

GRFs for scalable GPs. Reid et al. [4] previously suggested using graph random features for GPs, as part of a broader study of variance reduction techniques. However, their experiments focused

¹We consider GPs defined on the nodes of a *fixed* graph. The input space is finite and we perform inference for a finite set of random variables, one per node. The relationships between these variables are determined by the structure of \mathcal{G} via a graph node kernel. Whilst some might prefer to call this a ‘Gaussian random field’ or simply a ‘multivariate Gaussian’, in this paper we use ‘GP on a graph’ for consistency with recent literature [3], [4], [5].

exclusively on the diffusion kernel with small graphs, failing to fully exploit the estimator’s sparsity. Moreover, they limited their interest to computing the posterior, omitting any exploration of applications such as Bayesian optimisation.

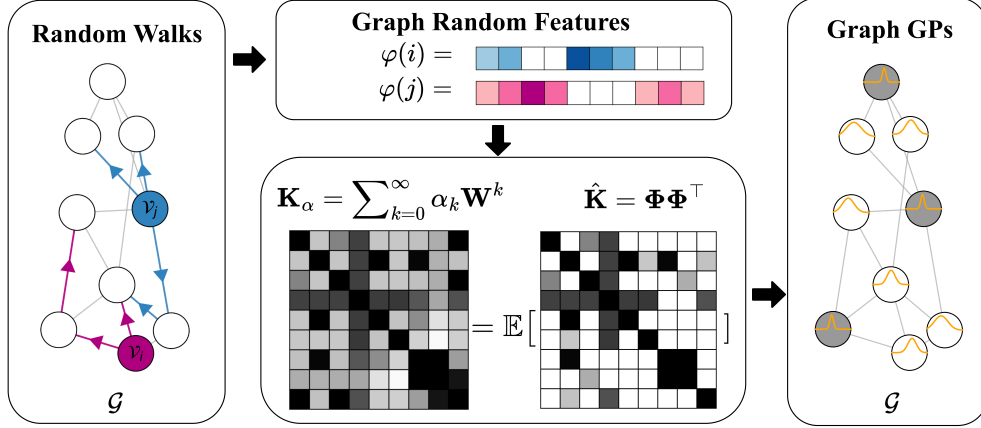


Figure 1: **GRFs for scalable GPs on graphs.** The GRFs algorithm constructs random features $\varphi(i)$ for nodes $i \in \{1, \dots, N\}$ using random walks. $\hat{\mathbf{K}} := [\varphi(i)^\top \varphi(j)]_{i,j=1}^N$ is an unbiased, sparse approximation of the kernel matrix \mathbf{K}_α , enabling efficient posterior inference in $\mathcal{O}(N^{3/2})$.

Key contributions. We perform the first detailed study of graph random features (GRFs) for Gaussian processes (GPs), unlocking robust, scalable Bayesian inference on graphs with $> 1\text{M}$ nodes.

1. We use GRFs to construct sparse estimates of learnable graph node kernels, and use these as covariance functions for GPs. Figure 1 gives a schematic.
2. We prove that Bayesian inference with GRFs enjoys $\mathcal{O}(N^{3/2})$ time complexity, compared to $\mathcal{O}(N^3)$ for exact alternatives. We confirm the time complexity empirically. In experiments, this translates to $50 \times$ wall-clock speedups on graphs with fewer than 10K nodes. Remarkably, the expressiveness and flexibility of GRFs enables them to outperform dense alternatives on test MSE.
3. We showcase our new techniques by performing Bayesian optimisation on massive graphs, implementing Thompson sampling with $> 1\text{M}$ nodes on a single computer chip.²

2 Preliminaries

Consider an undirected graph $\mathcal{G} = (\mathcal{V}, \mathcal{E}, \mathbf{W})$, consisting of a set of nodes $\mathcal{V} = \{1, \dots, N\}$, a set of edges $\mathcal{E} \subseteq \mathcal{V} \times \mathcal{V}$, and a weighted adjacency matrix $\mathbf{W} \in \mathbb{R}^{N \times N}$. Here $\mathbf{W}_{ij} = 0$ if $(i, j) \notin \mathcal{E}$. Define the *graph Laplacian* $\mathbf{L} = \mathbf{D} - \mathbf{W}$, with $\mathbf{D} = \text{diag}(\sum_{j=1}^N \mathbf{W}_{ij})$. The *normalised* graph Laplacian is $\tilde{\mathbf{L}} := \mathbf{D}^{-1/2} \mathbf{L} \mathbf{D}^{-1/2}$, whose spectrum conveniently lies in $[0, 2]$ [11].

Graph node kernels. A graph node kernel is a symmetric, positive semidefinite function $k : \mathcal{V} \times \mathcal{V} \rightarrow \mathbb{R}$, mapping pairs of graph nodes to real numbers [2]. Heuristically, it assigns similarity scores to every pair, which are assembled into a *Gram matrix* $\mathbf{K} := [k(i, j)]_{i,j=1}^N \in \mathbb{R}^{N \times N}$. Many popular graph node kernels are parameterised as functions of \mathbf{W} , \mathbf{L} or $\tilde{\mathbf{L}}$, expressed using the power series

$$\mathbf{K}_\alpha(\mathbf{W}) = \sum_{k=0}^{\infty} \alpha_k \mathbf{W}^k, \quad \alpha_k \in \mathbb{R} \quad \forall k \in (0, 1, \dots, \infty). \quad (1)$$

The set of coefficients $(\alpha_k)_{k=0}^{\infty}$ determines the behaviour of the kernel – e.g. whether it upweights long- or short-range interactions. For instance, the *graph diffusion kernel* $\mathbf{K}_{\text{diff}} := \exp(-\beta \mathbf{L})$ takes $\alpha_k = (-\beta)^k / k!$. Graph node kernels flexibly capture structural information about \mathcal{G} , providing a natural choice for the covariance matrix of Gaussian processes [3], [4].

²We will make code publicly available.

Gaussian processes. Let us now consider modelling functions $f : \mathcal{V} \rightarrow \mathbb{R}$ defined on the set of graph nodes. A common task is to identify the node that maximises f , e.g. the most influential social media user, or ‘patient zero’ in an epidemiological contact network. In particular, we may wish to solve $x^* = \arg \max_{x \in \mathcal{V}} f(x)$. Suppose we have access to a sequence of T noisy observations of the objective $y_t = f(x_t) + \varepsilon$, $\varepsilon \sim \mathcal{N}(0, \sigma_n^2)$, $t \in (1, 2, \dots, T)$ at distinct nodes $x_t \in \mathcal{V}$, where σ_n^2 is the noise variance. A common choice of statistical surrogate for the objective function f , for which we can perform analytic Bayesian inference given observations $\mathcal{D}_T = \{(x_t, y_t)\}_{t=1}^T$ (also denoted $\mathcal{D}_T = \{\mathbf{x}, \mathbf{y}\}$), is the *Gaussian process* (GP) [1]:

$$f(x) \sim \text{GP}(m(x), k(x, x')). \quad (2)$$

Here, $m(x)$ is the mean function and $k(x, x')$ the covariance function (‘kernel’). In our setting, the input domain consists of the nodes of a fixed graph. We can ‘train’ the kernel parameters $(\alpha_k)_{k=0}^\infty$ by optimising the *log-marginal likelihood* on the training data \mathcal{D}_T , and then compute the analytic posterior mean and covariance:

$$m_{|\mathbf{y}}(x) = m(x) + k(x, \mathbf{x})[k(\mathbf{x}, \mathbf{x}) + \sigma_n^2 \mathbf{I}]^{-1}(\mathbf{y} - m(\mathbf{x})), \quad (3)$$

$$k_{|\mathbf{y}}(x, x') = k(x, x') - k(x, \mathbf{x})[k(\mathbf{x}, \mathbf{x}) + \sigma_n^2 \mathbf{I}]^{-1}k(\mathbf{x}, x'). \quad (4)$$

Bayesian optimisation (BO) [12], [13] uses the posterior mean and variance – or related quantities, like samples from the posterior – to efficiently locate x^* in the presence of uncertainty. It trades off exploration and exploitation in a mathematically principled manner, helping us decide which node to query next in our attempt to maximise f .

Efficiency and scalability. A core computational challenge with performing Bayesian inference on graphs using GPs is that even just *evaluating* a dense graph kernel \mathbf{K}_α generally incurs $\mathcal{O}(N^3)$ time complexity, let alone computing the matrix-vector products and matrix inversions that we will in general require for BO. This is because it involves evaluating functions like $\exp(\cdot)$ or $(\cdot)^{-1}$ of the $N \times N$ weighted adjacency matrix \mathbf{W} , which becomes expensive for big graphs. For Euclidean kernels, a common recourse to improve scalability is to use *random features* [14], [15], [16]: stochastic, finite-dimensional features $\{\varphi(i)\}_{i=1}^N \in \mathbb{R}^m$ whose dot product is equal to the true kernel evaluation in expectation, $k(i, j) = \mathbb{E}(\varphi(i)^\top \varphi(j))$. In close analogy for discrete domains, researchers recently introduced *graph random features* (GRFs) [6], [7] – sparse random walk-based vectors for unbiased estimation of graph node kernels.

Graph random features: sparse, sharp kernel estimators using random walks. The mathematical details of GRFs are involved and can be safely omitted on a first reading, but their behaviour can be intuitively understood as follows. Consider a sequence of scalars $(f_k)_{k=0}^\infty$ satisfying $\sum_{k=0}^i f_k f_{i-k} = \alpha_i \forall i$ – namely, the ‘deconvolution’ of $(\alpha_i)_{i=0}^\infty$. We will refer to f_k as the *modulation function*. Suppose that the power series $\Psi := \sum_{k=0}^\infty f_k \mathbf{W}^k$ converges. Then it is straightforward to see that for symmetric \mathbf{W} (undirected graphs), we have that $\Psi^\top \Psi = \mathbf{K}_\alpha$. Recall that powers of an adjacency matrix count walks on a graph: for instance, \mathbf{W}_{ij}^k gives the (weighted) number of walks of length k between nodes i and j . Since \mathbf{K} converges, longer walks must eventually be discounted, either due to decaying f_k or due to multiplication of edge weights that are less than 1. The key insight of GRFs is that we can compute a Monte Carlo estimate $\Phi \in \mathbb{R}^{N \times N}$ that satisfies $\Psi = \mathbb{E}(\Phi)$ by importance sampling random walks.

Concretely, we simulate random walks out of every node of the graph. Each random walk consists of a number of ‘prefix subwalks’ – namely, the sequence given by the first `length(prefix_subwalk)` nodes visited. We keep track of 1) the weights of edges they traverse, 2) the modulation function f , and 3) their marginal probabilities. Using a simple formula, we can construct unbiased,³ sparse N -dimensional vectors that satisfy $\mathbb{E}(\varphi(i)^\top \varphi(j)) = \mathbb{E}([\Phi \Phi^\top]_{ij}) = [\mathbf{K}_\alpha]_{i,j}$. Alg.1 below provides pseudocode. It is deliberately kept high-level for compactness; the interested reader can find more details in Section B.

³It has been noted that the shared source of randomness actually introduces a $\mathcal{O}(1/n)$ bias term for estimates of diagonal kernel entries \mathbf{K}_{ii} . This is of little significance for large graphs with many walkers so, following convention [6], [7], we omit further discussion. One *could* remove this bias by sampling two independent ensembles of random walks and taking $\hat{\mathbf{K}} = \Phi_1 \Phi_2^\top$, at the cost of losing the positive definiteness guarantee and thus worse performance.

Algorithm 1: Constructing a GRF vector $\varphi(i) \in \mathbb{R}^N$ to approximate $\mathbf{K}_\alpha(\mathbf{W})$

```

1 Inputs: weighted graph  $\mathcal{G}$ , modulation function  $f : \mathbb{N} \rightarrow \mathbb{R}$ , random walk sampler  $p$ .
2 Output: Set of sparse GRFs  $\{\varphi(i)\}_{i=1}^N \in \mathbb{R}^N$  that satisfy  $\mathbf{K}_{ij} = \mathbb{E}(\varphi(i)^\top \varphi(j))$ .
3 for  $i \in \mathcal{V}$ :
4   initialise  $\varphi(i) \leftarrow \mathbf{0}$ 
5   for  $\text{walker\_idx} \in 1, \dots, n$ :
6     sample  $\text{random\_walk} \sim p$ 
7     for  $\text{prefix\_subwalk} \in \text{random\_walk}$ :
8        $\varphi(i)[\text{prefix\_subwalk}[-1]] +=$ 
9        $(\prod \text{traversed\_edge\_weights}) * \text{length}(\text{prefix\_subwalk}) / p(\text{prefix\_subwalk})$ 
10    normalise  $\varphi(i) / = n$ 

```

Remarkably, under mild assumptions on \mathcal{G} and (α_i) , GRFs provide very sharp estimates of \mathbf{K}_α . In particular, the estimates satisfy exponential concentration bounds, whilst storing only $\mathcal{O}(1)$ nonzero entries per feature. See Theorem 1 for a formal statement. As we will see in Section 3, we can use the sparse kernel estimate $\hat{\mathbf{K}} := \Phi\Phi^\top$ as an efficient alternative to the dense exact kernel \mathbf{K}_α , speeding up inference from $\mathcal{O}(N^3)$ to $\mathcal{O}(N^{3/2})$.

3 Scalable posterior inference with GRFs

In this section, we demonstrate how GRFs speed up posterior inference. We begin by proving novel theoretical results (Section 3.1), and then describe how they are used in our full efficient GP workflow (Section 3.2), enabling full posterior inference in $\mathcal{O}(N^{3/2})$ time.

3.1 Novel theoretical results

We first recall a seminal result for GRFs, proved by Reid et al. [4].

Theorem 1. (GRFs are sparse and give sharp kernel estimates [4]). Consider a graph \mathcal{G} with a weighted adjacency matrix \mathbf{W} and node degrees $\{d_i\}_{i=1}^N$. Suppose we sample GRFs $\{\varphi(i)\}_{i=1}^N$ by sampling n random walks that terminate with probability p at each timestep, with modulation function f . Suppose also that $c := \sum_{k=0}^{\infty} |f_k| \left(\max_{i,j \in [1,N]} \mathbf{W}_{ij} d_i / (1-p) \right)^k$ is finite. Then we have that

$$\mathbb{P}(|\varphi(i)^\top \varphi(j) - \mathbf{K}_{ij}| > t) \leq 2 \exp\left(-\frac{t^2 n^3}{2(2n-1)^2 c^4}\right). \quad (5)$$

Moreover, with probability at least $1 - \delta$, any GRF $\varphi(i)$ has $n \log(1 - (1 - \delta)^{1/n}) \log(1 - p)^{-1}$ or fewer nonzero entries.

Proof. The full proof, which uses McDiarmid’s inequality, is reported by Reid et al. [4]. ■

Theorem 1 demonstrates that, despite being sparse, GRFs give sharp kernel estimates. In particular, we can use Eq. (5) to compute the number of walkers n needed to guarantee an accurate estimate of \mathbf{K} with high probability. Because of the bound, this number is *independent of the graph size N* . n then determines the number of nonzero entries in the GRF, which also inherits independence of graph size N .

We note that Theorem 1 makes the mild assumption about the graph \mathcal{G} that the constant c is finite. This is not controversial; Reid et al. [10] provide extensive discussion. Intuitively, it is natural that the spectrum of \mathbf{W} must lie in some radius of convergence in order for the power series $\sum_{k=0}^{\infty} \alpha_k \mathbf{W}^k$ to converge. The condition for its Monte Carlo estimate to converge is only slightly stronger. Pragmatically, for computational reasons we only sample random walks up to some fixed maximum length

i_{\max} , whereupon $f_i = 0 \forall i > i_{\max}$. The condition thus trivially holds in all our experiments – or indeed any reasonable implementation.

With Theorem 1 in mind, we will henceforth assume that the number of walkers n is constant, safe in the knowledge that this gives a sharp kernel estimate. To the best of our knowledge, Property (2) of Theorem 2 is novel.

Theorem 2. (Properties of $\hat{\mathbf{K}}$). The randomised approximate Gram matrix $\hat{\mathbf{K}} := \Phi\Phi^\top = [\varphi(i)^\top\varphi(j)]_{i,j=1}^N \in \mathbb{R}^{N \times N}$ has the following properties.

1. *Property 1.* $\hat{\mathbf{K}}$ supports $\mathcal{O}(N)$ matrix-vector multiplication;
2. *Property 2.* The condition number of the approximate Gram matrix $\kappa(\hat{\mathbf{K}} + \sigma_n^2\mathbf{I})$ is $\mathcal{O}(N)$.

Proof. Property (1) follows trivially from the fact that $\hat{\mathbf{K}}$ has $\mathcal{O}(N)$ nonzero entries, whereupon matrix-vector multiplication only requires $\mathcal{O}(N)$ operations. Considering (2), since $\hat{\mathbf{K}}$ is positive definite, the smallest possible eigenvalue of $\hat{\mathbf{K}} + \sigma_n^2\mathbf{I}$ is σ_n^2 . Then note that

$$\|\hat{\mathbf{K}}\|_2 \leq \|\hat{\mathbf{K}}\|_F := \sqrt{\sum_{i,j=1}^N |\hat{\mathbf{K}}_{i,j}|^2} = \sqrt{\sum_{i,j=1}^N |\varphi(i)^\top\varphi(j)|^2} \leq N \max_{i,j} |\varphi(i)^\top\varphi(j)|. \quad (6)$$

Under the assumptions above $\|\varphi(i)\|_1 \leq c \forall i$, whereupon $|\varphi(i)^\top\varphi(j)| \leq c^2 \forall i, j$. Hence, we have that $\kappa(\hat{\mathbf{K}} + \sigma_n^2\mathbf{I}) \leq 1 + N \frac{c^2}{\sigma_n^2}$, which is $\mathcal{O}(N)$ as claimed. ■

Theorem 2 immediately implies the following corollary.

Lemma 1. Solving the sparse linear system is $\mathcal{O}(N^{3/2})$. Consider solving the system $(\hat{\mathbf{K}} + \sigma_n^2\mathbf{I})\mathbf{v} = \mathbf{b}$, where $\mathbf{v}, \mathbf{b} \in \mathbb{R}^N$. This can be achieved with the conjugate gradient method in time $\mathcal{O}(N^{3/2})$.

Proof. Using the conjugate gradient method, it is known that the system can be solved in $\sqrt{\kappa(\hat{\mathbf{K}} + \sigma_n^2\mathbf{I})}$ iterations [17], which by property (2) above is $\mathcal{O}(N^{1/2})$. Each iteration involves matrix-vector multiplication, which is $\mathcal{O}(N)$ in our case due to property (1). Combining gives a total time complexity of $\mathcal{O}(N^{3/2})$. ■

We remark that this is substantially less than the $\mathcal{O}(N^3)$ time complexity of exact GP methods that use \mathbf{K} rather than $\hat{\mathbf{K}}$. It is also straightforward to see that Theorem 2 and Lemma 1 will continue to hold if we only consider a subset of the nodes of the graph, e.g. just considering a set of training nodes of cardinality $N_{\text{train}} \leq N$.

3.2 From pathwise conditioning to conjugate gradients: efficient posterior inference with GRFs

We now introduce the ‘cookbook’ of posterior inference on graphs using GRFs in three steps: kernel initialisation, hyperparameters learning and posterior inference. We will also analyse the overall time and space complexity of this workflow.

Kernel initialisation. We compute the Gram matrix using the procedure in Alg.1, which involves sampling n random walks for every node on the graph. This yields a sparse kernel approximation:

$$\hat{\mathbf{K}} := \Phi\Phi^\top = [\varphi(i)^\top\varphi(j)]_{i,j=1}^N \in \mathbb{R}^{N \times N}. \quad (7)$$

Note that, in practice, $\hat{\mathbf{K}}$ does not need to be materialised, as we can replace the matrix-vector product $\hat{\mathbf{K}}\mathbf{v}$ with two fast matrix-vector products $\Phi(\Phi^\top\mathbf{v})$. Each is computed in linear time.

Hyperparameter learning. Denote the training data $\mathcal{D}_T = \{\mathbf{x}, \mathbf{y}\}$ containing training nodes \mathbf{x} and corresponding noisy observations \mathbf{y} . We learn the hyperparameters θ , such as observation noise and the modulation function f , by maximising the log marginal likelihood,

$$\mathcal{L}(\theta) = -\frac{1}{2}\mathbf{y}^\top\mathbf{H}_\theta^{-1}\mathbf{y} - \frac{1}{2}\log\det(\mathbf{H}_\theta) - \frac{N}{2}\log(2\pi), \quad (8)$$

where $\mathbf{H}_\theta = (\hat{\mathbf{K}}_{\mathbf{x}\mathbf{x}} + \sigma_n^2\mathbf{I})$. In particular, we use the Adam optimiser and estimate the gradient,

$$\nabla \mathcal{L}(\theta) = \frac{1}{2} (\mathbf{H}_\theta^{-1} \mathbf{y})^\top \frac{\partial \mathbf{H}_\theta}{\partial \theta} (\mathbf{H}_\theta^{-1} \mathbf{y}) - \frac{1}{2} \text{tr} \left(\mathbf{H}_\theta^{-1} \frac{\partial \mathbf{H}_\theta}{\partial \theta} \right), \quad (9)$$

using iterative methods [18], [19]. These avoid explicit matrix inverses via iterative linear system solvers such as conjugate gradients (CGs) [17], [20]. Since CGs rely on matrix-vector multiplication, this allows us to leverage the efficient structure of our GRFs kernel. Meanwhile, the trace term is estimated using Hutchinson’s trace estimator [21],

$$\text{tr} \left(\mathbf{H}_\theta^{-1} \frac{\partial \mathbf{H}_\theta}{\partial \theta} \right) = \mathbb{E} \left(\mathbf{z}^\top \mathbf{H}_\theta^{-1} \frac{\partial \mathbf{H}_\theta}{\partial \theta} \mathbf{z} \right) \approx \frac{1}{S} \sum_{s=1}^S \mathbf{z}_s^\top \mathbf{H}_\theta^{-1} \frac{\partial \mathbf{H}_\theta}{\partial \theta} \mathbf{z}_s, \quad (10)$$

where \mathbf{z}_s are random probe vectors satisfying $\mathbb{E} [\mathbf{z}_s \mathbf{z}_s^\top] = \mathbf{I}$. This leads to a batch of linear systems,

$$\mathbf{H}_\theta [\mathbf{v}_y, \mathbf{v}_1, \dots, \mathbf{v}_S] = [\mathbf{y}, \mathbf{z}_1, \dots, \mathbf{z}_S], \quad (11)$$

which can be solved via iterative linear system solvers, and whose solutions allow us to estimate $\nabla \mathcal{L}$.

Posterior Inference. We perform posterior inference using a combination of pathwise conditioning [22], [23] and iterative methods. This combination has previously been used by Lin et al. [24], [25] to leverage Kronecker-structured matrices, and it allows us to exploit our efficient GRFs structure. In particular, pathwise conditioning expresses a sample from the posterior as a sample from the prior with an additional correction term,

$$\mathbf{g}_{\mathbf{y}}(\cdot) = \mathbf{g}(\cdot) + \hat{\mathbf{K}}_{(\cdot)\mathbf{x}} \left(\hat{\mathbf{K}}_{\mathbf{x}\mathbf{x}} + \sigma_n^2 \mathbf{I} \right)^{-1} (\mathbf{y} - (\mathbf{g}(\mathbf{x}) + \varepsilon)), \quad (12)$$

where (\cdot) is any node on the graph \mathcal{G} , $\mathbf{g}_{\mathbf{y}}$ is a sample from the posterior, \mathbf{g} is a sample from the prior, and $\varepsilon \sim \mathcal{N}(\mathbf{0}, \sigma_n^2 \mathbf{I})$. This facilitates the use of iterative linear system solvers to compute $\left(\hat{\mathbf{K}}_{\mathbf{x}\mathbf{x}} + \sigma_n^2 \mathbf{I} \right)^{-1} (\mathbf{y} - (\mathbf{g}(\mathbf{x}) + \varepsilon))$, which again avoids the explicit inverse and leverages sparse matrix multiplication. Again, we use CGs [17], [20] as linear system solver, though alternatives have been proposed recently [26], [27]. The structure of the GRFs kernel also admits efficient sampling from the prior via $\mathbf{g} = \Phi \mathbf{w}$ with $\mathbf{w} \sim \mathcal{N}(\mathbf{0}, \mathbf{I})$,⁴ since $\text{Cov}(\Phi \mathbf{w}) = \Phi \Phi^\top = \hat{\mathbf{K}}$.

Algorithm complexity. Kernel initialisation takes $\mathcal{O}(N)$ time, since a fixed number of random walks are simulated all N nodes. Training and inference are dominated by solving sparse linear systems with CGs, which has $\mathcal{O}(N^{3/2})$ time complexity (Lemma 1). All stages use sparse matrices (e.g. $\hat{\mathbf{K}} + \sigma_n^2 \mathbf{I}$) with $\mathcal{O}(N)$ nonzero entries, giving overall space complexity $\mathcal{O}(N)$.

4 Experimental results

Here, we present empirical results demonstrating the scalability and practical effectiveness of the GRF-GPs model. Full experimental details are provided in App. C.

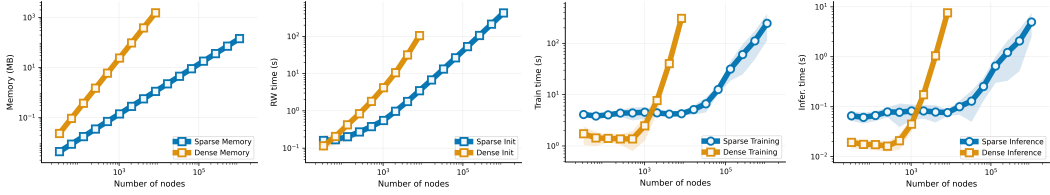
4.1 Scalable posterior inference on graphs

We begin by examining empirical time and space complexity, before applying the method to real-world regression task, following the setup of Borovitskiy et al. [3].

Time and space complexity measurements. We benchmark posterior inference on synthetic graphs under two GRFs implementations: a dense baseline (explicit adjacency materialisation) and a sparse variant that exploits GRFs sparsity. The full measurements are in Table 3 and Table 4. For a graph with 8192 nodes, we observe a **50× speedup** in total wall-clock time.

Figure 2 shows scaling curves, plotted log–log scale, with exponents from the asymptotic regime given in Table 1. As expected, the GRFs method attains **linear** memory and initialisation cost, and **sub-quadratic** training and inference, scaling to graphs with **1M nodes**. The near-linear runtime trends in training and inference reflect the fixed iteration budget of sparse linear solves; conditioning effects have not yet dominated at these scales.

⁴Here, \mathbf{g} is an N -dimensional vector corresponding to a sample evaluated at all N nodes. One could also consider a subset of nodes, whereupon the prior sample at a specific node $\mathbf{g}(\cdot)$ corresponds to the vector’s (\cdot) th entry.



(a) Memory usage (b) Initialisation time (c) Training wall-clock time (d) Inference wall-clock time

Figure 2: **GRFs scale better (blue curve) when sparsity is leveraged.** Scaling experiments for the GRF-GPs. Yellow curves: brute-force dense implementation. Blue curves: sparse implementation. Panels (a)–(d) correspond to memory footprint, training time, kernel initialisation time and inference time, respectively. The dense model is limited to 8,192 nodes due to its higher memory demands.

Table 1: **GRFs have sub-quadratic time scaling and linear memory scaling.** Empirical scaling coefficients for memory usage, kernel initialisation time, training time, and inference time with respect to graph size N . A factor b indicates scaling $\mathcal{O}(N^b)$.

Kernel	Memory	Kernel init. time	Training time	Inference time
GRFs (Dense)	2.00	1.21	1.97	2.16
GRFs (Sparse)	1.00	0.81	1.04	1.04

Regression task: traffic speed prediction. To assess predictive utility, we now apply GRF-GPs to a traffic speed forecasting task (Figure 5) on the San Jose freeway sensor network [28]. We compare predictive accuracy across kernel types. This experiment demonstrates that the flexibility of the GRFs modulation function yields improved predictive accuracy. Beyond this expressivity, GRFs can also outperform exact kernels due to their inherently sparse structure, which encodes a meaningful inductive bias: predictions for a node depend predominantly on information from its local neighborhood. In contrast, traditional dense kernels are prone to the “oversmoothing” effect as they capture spurious long-range correlations driven by noise [29].

We compare three kernel configurations by measuring the relative L_2 error between maximum-a-posteriori (MAP) predictions (posterior means) and the ground-truth traffic speed. GRFs kernels are computed with different numbers of random walkers n to examine the trade-off between accuracy and computational budget:

Exact Diffusion : $\mathbf{K}_{\text{diff}} = \exp(-\beta\mathbf{L})$,

Diffusion-shape $\hat{\mathbf{K}}$: $f_k = \frac{\beta^k}{k!}$,

General $\hat{\mathbf{K}}$: f_k learned directly.

Figure 3 reports the relative L_2 error as a function of the number of random walks per node n . As n increases, $\hat{\mathbf{K}}$ better captures the underlying graph structure, yielding more accurate predictions. The general GRFs kernel consistently outperforms the diffusion-shaped variant, highlighting the benefit of learning a flexible modulation function. Because the GRFs kernel’s modulation function has greater degrees of freedom than the exact diffusion kernel, it is more expressive and can model the data more effectively when enough walks are used. For $n \gtrsim 1000$, the general GRFs kernel surpasses the exact diffusion baseline.

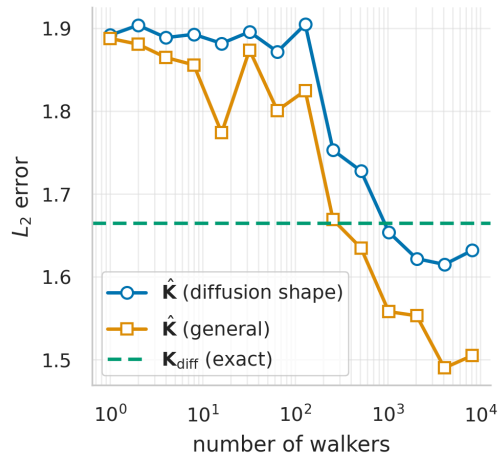


Figure 3: **GRFs kernels outperform diffusion kernel when $n \gtrsim 1000$.** Average relative L_2 error vs. number of walks per node n on the San Jose traffic network. Blue: GRFs with diffusion-shaped modulation function. Orange: GRFs with directly-learned modulation function. Green dashed: exact diffusion kernel.

4.2 Scalable and robust Bayesian optimisation

Leveraging GRFs’ scalability, we now apply the model to Bayesian optimisation (BO) on a graph with 10^6 nodes. We use Thompson Sampling as the acquisition strategy, drawing samples from the posterior over the objective function and selecting maximisers [30], [31]. Posterior sampling is made efficient by pathwise conditioning, given in Equation (12).

We compare against random search and breadth-first search (BFS) across four synthetic graph benchmarks. Figure 4 shows that GRFs-based BO achieves lower regret than search-based baselines in most datasets, highlighting the advantage of uncertainty-aware strategies for large-scale graph optimisation. Performance gains were most pronounced on multimodal and periodic landscapes, where naive search strategies struggled to escape local optima.

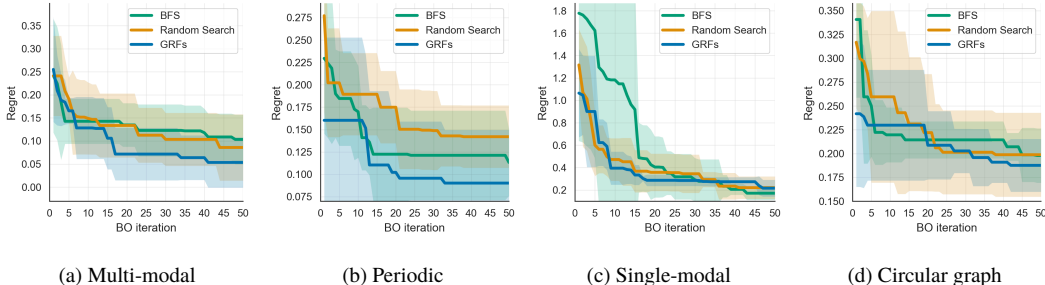


Figure 4: **GRFs-based BO achieves lower regret than search-based baselines in most datasets.** Regret curves for Bayesian Optimisation on synthetic graphs with 10^6 nodes. We evaluate four synthetic benchmark: (a) multi-modal, (b) periodic, (c) single-modal, and (d) circular graph. Our GRFs-based Thompson Sampling approach is compared against random search and BFS baselines. Shaded regions indicate ± 1 standard deviation across 5 runs.

4.3 Future work: scalable variational GP for classification

We evaluate GRF-GPs on a multi-class node classification task using the Cora citation network benchmark [32]. In this non-conjugate inference setting, we handle the non-Gaussian likelihood via variational inference [33]. Pathwise conditioning for classification is nontrivial [23]; we defer a full treatment to future work. Instead, we use a brute-force GRFs implementation, which clearly shows the empirical effectiveness of our method but does not yet have explicit time complexity guarantees.

We compare classification performance across exact and GRFs kernel configurations. Our experiments use an 80/20 train–test split on the largest connected component of the graph. Experiment details can be found in Section C.4. Table 2 reports classification accuracies.

Table 2: **The GRFs kernel reaches highest accuracy in the Cora benchmark.** Classification accuracy on the Cora dataset with different graph kernels. With $n = 16384$ walks per node (22.17% non-zero entries), the GRFs kernel outperforms both diffusion and Matérn kernels.[3].

Kernel	Form	Accuracy
Diffusion	$\mathbf{K}_{\text{diff}} = \exp(-\beta\mathbf{L})$	$85.31 \pm 0.61\%$
GRFs	$\hat{\mathbf{K}} = \Phi\Phi^\top$	$87.04 \pm 0.53\%$
Matérn	$\mathbf{K}_{\text{Matérn}} = \left(\frac{2\nu}{\kappa^2} + \tilde{\mathbf{L}}\right)^{-\nu}$	$86.72 \pm 0.31\%$

5 Conclusion

We have demonstrated how graph random features (GRFs), a recently-introduced Monte Carlo algorithm, can be used to speed up training and inference with Gaussian processes on discrete input spaces. Under mild assumptions, GRFs support $\mathcal{O}(N^{3/2})$ time complexity inference – much faster than $\mathcal{O}(N^3)$ for their exact counterpart. This translates to substantial wall-clock time speedups, and unlocks scalable Bayesian optimisation on massive topologies with little sacrifice in performance.

- [1] C. E. Rasmussen, “Gaussian processes in machine learning,” *Summer school on machine learning*. Springer, pp. 63–71, 2003.
- [2] A. J. Smola and R. Kondor, “Kernels and regularization on graphs,” in *Learning theory and kernel machines: 16th annual conference on learning theory and 7th kernel workshop, COLT/kernel 2003, Washington, DC, USA, august 24-27, 2003. Proceedings*, 2003, pp. 144–158.
- [3] V. Borovitskiy, I. Azangulov, A. Terenin, P. Mostowsky, M. Deisenroth, and N. Durrande, “Matérn Gaussian processes on graphs,” in *International Conference on Artificial Intelligence and Statistics*, 2021, pp. 2593–2601.
- [4] I. Reid, S. Markou, K. Choromanski, R. E. Turner, and A. Weller, “Variance-Reducing Couplings for Random Features,” *arXiv preprint arXiv:2405.16541*, 2024.
- [5] X. Wan, P. Osselin, H. Kenlay, B. Ru, M. A. Osborne, and X. Dong, “Bayesian optimisation of functions on graphs,” *Advances in Neural Information Processing Systems*, vol. 36, pp. 43012–43040, 2023.
- [6] K. M. Choromanski, “Taming graph kernels with random features,” in *International Conference on Machine Learning*, 2023, pp. 5964–5977.
- [7] I. Reid, K. Choromanski, E. Berger, and A. Weller, “General graph random features,” *arXiv preprint arXiv:2310.04859*, 2023.
- [8] J. S. Hendricks and T. E. Booth, “MCNP variance reduction overview,” in *Monte-Carlo Methods and Applications in Neutronics, Photonics and Statistical Physics: Proceedings of the Joint Los Alamos National Laboratory-Commissariat à l’Energie Atomique Meeting Held at Cadarache Castle, Provence, France April 22–26, 1985*, 2006, pp. 83–92.
- [9] L. L. Carter and E. D. Cashwell, “Particle-transport simulation with the Monte Carlo method,” 1975.
- [10] I. Reid *et al.*, “Linear transformer topological masking with graph random features,” *arXiv preprint arXiv:2410.03462*, 2024.
- [11] F. R. Chung, *Spectral graph theory*, vol. 92. American Mathematical Soc., 1997.
- [12] J. Močkus, “On Bayesian methods for seeking the extremum,” in *IFIP Technical Conference on Optimization Techniques*, 1974, pp. 400–404.
- [13] D. R. Jones, M. Schonlau, and W. J. Welch, “Efficient global optimization of expensive black-box functions,” *Journal of Global optimization*, vol. 13, no. 4, pp. 455–492, 1998.
- [14] A. Rahimi and B. Recht, “Random features for large-scale kernel machines,” *Advances in neural information processing systems*, vol. 20, 2007.
- [15] J. Yang, V. Sindhwani, Q. Fan, H. Avron, and M. W. Mahoney, “Random laplace feature maps for semi-group kernels on histograms,” in *Proceedings of the IEEE Conference on Computer Vision and Pattern Recognition*, 2014, pp. 971–978.
- [16] F. X. X. Yu, A. T. Suresh, K. M. Choromanski, D. N. Holtmann-Rice, and S. Kumar, “Orthogonal random features,” *Advances in neural information processing systems*, vol. 29, 2016.
- [17] J. R. Shewchuk, “An Introduction to the Conjugate Gradient Method Without the Agonizing Pain,” 1994.
- [18] J. Gardner, G. Pleiss, K. Q. Weinberger, D. Bindel, and A. G. Wilson, “GPYtorch: Blackbox Matrix-Matrix Gaussian Process Inference with GPU Acceleration,” in *Advances in Neural Information Processing Systems*, 2018.
- [19] J. A. Lin, S. Padhy, B. Mlodozieniec, J. Antorán, and J. M. Hernández-Lobato, “Improving Linear System Solvers for Hyperparameter Optimisation in Iterative Gaussian Processes,” in *Advances in Neural Information Processing Systems*, 2024.
- [20] M. R. Hestenes and E. Stiefel, “Methods of Conjugate Gradients for Solving Linear Systems,” *Journal of Research of the National Bureau of Standards*, vol. 49, no. 6, 1952.
- [21] M. Hutchinson, “A Stochastic Estimator of the Trace of the Influence Matrix for Laplacian Smoothing Splines,” *Communications in Statistics - Simulation and Computation*, vol. 19, no. 2, 1990.
- [22] J. T. Wilson, V. Borovitskiy, A. Terenin, P. Mostowsky, and M. P. Deisenroth, “Efficiently Sampling Functions from Gaussian Process Posteriors,” in *International Conference on Machine Learning*, 2020.
- [23] J. T. Wilson, V. Borovitskiy, A. Terenin, P. Mostowsky, and M. P. Deisenroth, “Pathwise Conditioning of Gaussian Processes,” *Journal of Machine Learning Research*, vol. 22, no. 1, 2021.

- [24] J. A. Lin, S. Ament, M. Balandat, and E. Bakshy, “Scaling Gaussian Processes for Learning Curve Prediction via Latent Kronecker Structure,” in *NeurIPS Bayesian Decision-making and Uncertainty Workshop*, 2024.
- [25] J. A. Lin, S. Ament, M. Balandat, D. Eriksson, J. M. Hernández-Lobato, and E. Bakshy, “Scalable Gaussian Processes with Latent Kronecker Structure,” in *International Conference on Machine Learning*, 2025.
- [26] J. A. Lin, J. Antorán, S. Padhy, D. Janz, J. M. Hernández-Lobato, and A. Terenin, “Sampling from Gaussian Process Posteriors using Stochastic Gradient Descent,” in *Advances in Neural Information Processing Systems*, 2023.
- [27] J. A. Lin *et al.*, “Stochastic Gradient Descent for Gaussian Processes Done Right,” in *International Conference on Learning Representations*, 2024.
- [28] C. Chen, K. Petty, A. Skabardonis, P. Varaiya, and Z. Jia, “Freeway Performance Measurement System: Mining Loop Detector Data,” in *80th Annual Meeting of the Transportation Research Board*, Washington, D.C., 2001. [Online]. Available: https://people.eecs.berkeley.edu/~varaiya/papers_ps.dir/MiningLoopDetectorData.pdf
- [29] N. Keriven, “Not too little, not too much: A theoretical analysis of graph (over)smoothing,” in *Advances in Neural Information Processing Systems*, 2022.
- [30] W. R. Thompson, “On the likelihood that one unknown probability exceeds another in view of the evidence of two samples,” *Biometrika*, vol. 25, no. 3–4, pp. 285–294, 1933.
- [31] D. J. Russo, B. Van Roy, A. Kazerouni, I. Osband, and Z. Wen, “A Tutorial on Thompson Sampling,” *Foundations and Trends® in Machine Learning*, vol. 11, no. 1, pp. 1–96, 2018, doi: 10.1561/22000000070.
- [32] A. McCallum, K. Nigam, J. Rennie, and J. Seymore, “Automating the Construction of Internet Portals with Machine Learning,” *Information Retrieval*, vol. 3, no. 2, pp. 127–163, 2000.
- [33] F. Leibfried, V. Dutoird, S. T. John, and N. Durrande, “A Tutorial on Sparse Gaussian Processes and Variational Inference.” [Online]. Available: <https://arxiv.org/abs/2012.13962>
- [34] A. G. d. G. Matthews *et al.*, “GPflow: A Gaussian process library using TensorFlow,” *Journal of Machine Learning Research*, vol. 18, no. 40, pp. 1–6, Apr. 2017, [Online]. Available: <http://jmlr.org/papers/v18/16-537.html>
- [35] M. van der Wilk, V. Dutoird, S. John, A. Artemev, V. Adam, and J. Hensman, “A Framework for Interdomain and Multioutput Gaussian Processes,” *arXiv:2003.01115*, 2020, [Online]. Available: <https://arxiv.org/abs/2003.01115>
- [36] K. A. Wang, G. Pleiss, J. R. Gardner, S. Tyree, K. Q. Weinberger, and A. G. Wilson, “Exact Gaussian Processes on a Million Data Points,” in *Advances in Neural Information Processing Systems*, 2019.

A Funding and acknowledgements

JAL is supported by the University of Cambridge Harding Distinguished Postgraduate Scholars Programme. AW acknowledges support from EPSRC via a Turing AI Fellowship under grant EP/V025279/1, and project FAIR under grant EP/V056883/1; and from the Leverhulme Trust via CFI. RET is supported by the EPSRC Probabilistic AI Hub (EP/Y028783/1). IR gratefully acknowledges funding from Trinity College, Cambridge and from Google. This work was funded in part by an unrestricted gift from Huawei.

Trustworthy, scalable and robust machine learning for graphs. Much of graph-based machine learning research to date has focused on graph neural networks. Kernel methods provide an exciting alternative which is inherently more explainable. Our algorithms are applicable to a broad range of real world settings, including many tasks in social networks. We demonstrate strong scalability, efficiency and performance whilst retaining the benefits of explainability.

B Full GRFs Algorithm

To complement the pseudocode provided in Alg. 1, Alg. 2 provides a more detailed explanation of how one can estimate graph node kernels using graph random features (GRFs). The motivated

reader is invited to consult the works of Reid et al. [7] and Choromanski [6] for the original accounts, including further intuitions and a proof of unbiasedness.

Algorithm 2: Constructing a random feature vector $\varphi(i) \in \mathbb{R}^N$ to approximate $\mathbf{K}_\alpha(\mathbf{W})$

Inputs: weighted adjacency matrix $\mathbf{W} \in \mathbb{R}^{N \times N}$ for a graph G with N nodes, vector of
1 unweighted node degrees $\mathbf{d} \in \mathbb{R}^N$, modulation function $f : (\mathbb{N} \cup \{0\}) \rightarrow \mathbb{R}$, termination
probability $p_{\text{halt}} \in (0, 1)$, node $i \in \mathcal{N}$, number of random walks to sample $n \in \mathbb{N}$.
2 **Output:** random walk feature vector $\varphi(i) \in \mathbb{R}^N$.
3 initialise: $\varphi(i) \leftarrow \mathbf{0}$
4 **for** $w = 1, \dots, n$
5 | initialise: **load** $\leftarrow 1$
6 | initialise: **current_node** $\leftarrow 1$
7 | initialise: **terminated** $\leftarrow \text{False}$
8 | initialise: **walk_length** $\leftarrow 0$
9 | **while** **terminated** = **False** **do**
10 | | $\varphi(i)$ [**current_node**] $\leftarrow \varphi(i)$ [**current_node**] + **load** $\times f(\text{walk_length})$
11 | | **walk_length** = **walk_length**+1
12 | | **new_node** $\leftarrow \text{Unif}[\mathcal{N}(\text{current_node})]$ ▷ assign to one of neighbours
13 | | **load** $\leftarrow \text{load} \times \frac{d[\text{current_node}]}{1-p_{\text{halt}}} \times \mathbf{W}[\text{current_node}, \text{new_node}]$ ▷ update load
14 | | **current_node** $\leftarrow \text{new_node}$
15 | | **terminated** $\leftarrow (t \sim \text{Unif}(0, 1) < p_{\text{halt}})$ ▷ draw RV to decide on termination
16 | **end while**
17 **end for**
18 | normalise $\varphi(i) = \varphi(i)/m$

C Experiment Details

We provide additional experimental details in this section. All experiments were conducted on a single compute node equipped with an NVIDIA GeForce RTX 2080 Ti GPU (11 GB memory).

C.1 Time and space complexity measurements

This section reports experimental details for the scaling results reported in Figure 2 and Table 1.

Synthetic data. Synthetic signals were generated on ring graphs of increasing size ($N = 2^5, 2^6, \dots, 2^{20}$ nodes). Node observations were defined by smooth periodic functions on the ring with additive Gaussian noise ($\sigma_n^2 = 0.1$). For graphs larger than 8192 nodes, only sparse experiments were conducted, since dense adjacency matrices exceeded available GPU memory.

Random feature matrices Φ were constructed using 100 random walks per node, with halting probability $p_{\text{halt}} = 0.1$. Walks longer than 3 hops were truncated.

Measurements taken. For each graph size, and across 5 random seeds, we measured:

- **Memory footprint** of the random feature matrices Φ .
- **Random-walk preprocessing time** for constructing Φ .
- **Training wall-clock time**, measured as total optimizer runtime over 50 epochs.
- **Inference wall-clock time**, measured as posterior mean and covariance evaluation time on the test set.

The dense implementation used a GPflow kernel with explicit adjacency materialization, while the sparse implementation used a GPyTorch kernel with customized sparse linear operators to maximize efficiency [18], [34], [35]. The full empirical measurements are shown in Table 3 and Table 4.

Table 3: Memory and time measurements for sparse implementation: mean \pm standard deviation.

Graph size	Memory (MB)	Kernel init time (s)	Training time (s)	Inference time (s)
32	0.004 \pm 0.000	0.160 \pm 0.033	4.103 \pm 0.216	0.066 \pm 0.007
64	0.008 \pm 0.000	0.168 \pm 0.022	3.823 \pm 0.136	0.061 \pm 0.008
128	0.015 \pm 0.000	0.202 \pm 0.022	4.036 \pm 0.191	0.066 \pm 0.007
256	0.030 \pm 0.000	0.271 \pm 0.030	4.369 \pm 0.349	0.079 \pm 0.009
512	0.059 \pm 0.000	0.379 \pm 0.021	4.395 \pm 0.619	0.077 \pm 0.019
1024	0.118 \pm 0.000	0.552 \pm 0.024	4.549 \pm 0.593	0.082 \pm 0.014
2048	0.235 \pm 0.000	0.973 \pm 0.039	4.416 \pm 0.320	0.082 \pm 0.012
4096	0.470 \pm 0.000	1.790 \pm 0.028	4.185 \pm 0.252	0.078 \pm 0.015
8192	0.938 \pm 0.000	3.481 \pm 0.074	4.247 \pm 0.143	0.076 \pm 0.006
16384	1.876 \pm 0.000	6.764 \pm 0.052	5.117 \pm 0.518	0.100 \pm 0.016
32768	3.751 \pm 0.000	13.297 \pm 0.050	6.623 \pm 1.048	0.129 \pm 0.040
65536	7.501 \pm 0.000	26.569 \pm 0.063	12.566 \pm 1.188	0.254 \pm 0.061
131072	15.001 \pm 0.000	53.012 \pm 0.156	31.534 \pm 6.376	0.651 \pm 0.175
262144	30.000 \pm 0.000	105.901 \pm 0.514	60.488 \pm 17.849	1.216 \pm 0.443
524288	60.000 \pm 0.000	212.671 \pm 0.758	111.672 \pm 31.377	2.068 \pm 0.775
1048576	120.000 \pm 0.000	426.074 \pm 1.562	245.060 \pm 65.159	4.947 \pm 1.226

Table 4: Memory and time measurements for dense implementation: mean \pm standard deviation.

Graph size	Memory (MB)	Kernel init time (s)	Training time (s)	Inference time (s)
32	0.024 \pm 0.000	0.115 \pm 0.017	1.726 \pm 0.336	0.019 \pm 0.002
64	0.094 \pm 0.000	0.205 \pm 0.012	1.430 \pm 0.219	0.018 \pm 0.002
128	0.375 \pm 0.000	0.421 \pm 0.025	1.403 \pm 0.116	0.017 \pm 0.002
256	1.500 \pm 0.000	0.840 \pm 0.044	1.371 \pm 0.152	0.016 \pm 0.002
512	6.000 \pm 0.000	1.800 \pm 0.069	1.370 \pm 0.288	0.021 \pm 0.004
1024	24.000 \pm 0.000	4.189 \pm 0.204	2.465 \pm 0.595	0.045 \pm 0.006
2048	96.000 \pm 0.000	10.546 \pm 0.107	7.680 \pm 1.649	0.173 \pm 0.001
4096	384.000 \pm 0.000	31.749 \pm 1.246	40.376 \pm 4.080	1.043 \pm 0.006
8192	1536.000 \pm 0.000	104.839 \pm 2.026	307.188 \pm 35.938	7.572 \pm 0.000

Scaling factor estimation. We estimated empirical complexity exponents by fitting the measured runtime and memory curves to a power-law model,

$$y \approx aN^b,$$

using ordinary least squares in log–log space, where N is the number of graph nodes. Uncertainty in the slope b was quantified with 95% confidence intervals derived from the t -distribution. To capture asymptotic scaling behavior, fits were restricted to sufficiently large graphs: dense GP experiments were fit for $N \geq 2^9$, while sparse GP experiments were fit for $N \geq 2^{15}$. The fitted coefficients a and b , together with confidence intervals and R^2 values, are summarized in Table 5.

Table 5: Fitted power-law scaling coefficients for memory usage, random-walk initialization, training, and inference time. Each row reports multiplicative constant a , exponent b with 95% confidence interval, and coefficient of determination R^2 . Fits performed in log–log space.

	Kernel	a	b	95% CI (b)	R^2
Memory (MB)	Sparse	1.37×10^{-4}	1.00	[1.00, 1.00]	1.00
	Dense	2.29×10^{-5}	2.00	[2.00, 2.00]	1.00
RW init time (s)	Sparse	3.58×10^{-3}	0.81	[0.73, 0.88]	0.97
	Dense	1.22×10^{-3}	1.21	[1.09, 1.33]	0.99
Training time (s)	Sparse	1.32×10^{-4}	1.04	[0.96, 1.12]	1.00
	Dense	3.93×10^{-6}	1.97	[1.20, 2.73]	0.96
Inference time (s)	Sparse	2.79×10^{-6}	1.04	[0.93, 1.14]	0.99
	Dense	1.92×10^{-8}	2.16	[1.50, 2.81]	0.97

C.2 Regression task: traffic speed prediction

Here we provide further details of the regression experiment: predicting the traffic speeds in the San Jose freeway sensor network [28], following the setup of Boroviskiy et al. [3].

Kernel approximation with GRFs. We used two variants of GRFs kernel. The first GRFs kernel uses the diffusion-like modulation function $f(k) = \frac{\beta^k}{k!}$. This is a truncated power series expansion of the diffusion kernel, where the learnable hyperparameters are length scale β and kernel variance σ_k^2 . The second kernel directly learns the modulation coefficients $\{f_k\}_{k=0}^P$, which are initialized randomly and learned via log marginal likelihood. For both GRFs variants, we fix $p_{\text{halt}} = 0.1$ and truncate walks at a maximum length of 10, and vary the number of walks per node $n \in \{1, 10, \dots, 10^4\}$.

Regression task. We apply GP inference using the 250 labeled nodes as training data to predict traffic speeds at all 1,016 nodes in the network. The kernel hyperparameter and noise variance σ_n^2 are learned by maximizing the log marginal likelihood, using Adam. Posterior inference then yields the predicted mean \hat{g} and covariance $\hat{\Sigma}$ of the latent traffic speed function over the graph.

To quantify accuracy, we compute the relative L_2 error on the 75 test nodes between the true speeds \mathbf{y}^{test} and the MAP estimate $\hat{\mathbf{g}}^{\text{test}}$:

$$\text{Relative } L_2 \text{ error} = \frac{\|\hat{\mathbf{g}}^{\text{test}} - \mathbf{y}^{\text{test}}\|_2}{\|\mathbf{y}^{\text{test}}\|_2}.$$

The experiment is repeated five times with different random seeds to compute the average L_2 error.

Capturing global and local patterns. Using the visualization toolkits in Boroviskiy et al., we illustrate posterior inference results from the GRF-GPs on the San Jose traffic network in Figure 5. The left panel provides a global view over the full network, while the right panel zooms in on a specific highway junction. We observe that the inferred mean captures large-scale spatial variation across the network—speeds are higher on main freeway segments and lower in peripheral or downtown regions. Notably, in the zoomed-in view, the model successfully distinguishes speeds across tightly packed lanes running in opposite directions. Despite spatial proximity, the posterior assigns significantly different mean values to adjacent but directionally distinct segments, demonstrating that GRF-GPs inference captures connectivity-aware patterns rather than relying solely on Euclidean distance. The bottom row visualizes posterior uncertainty, with standard deviation plotted over the full graph (left) and zoomed in (right). These results confirm that GRF-GPs respect both global graph structure and local topology, delivering interpretable and spatially coherent predictions on complex, real-world networks.

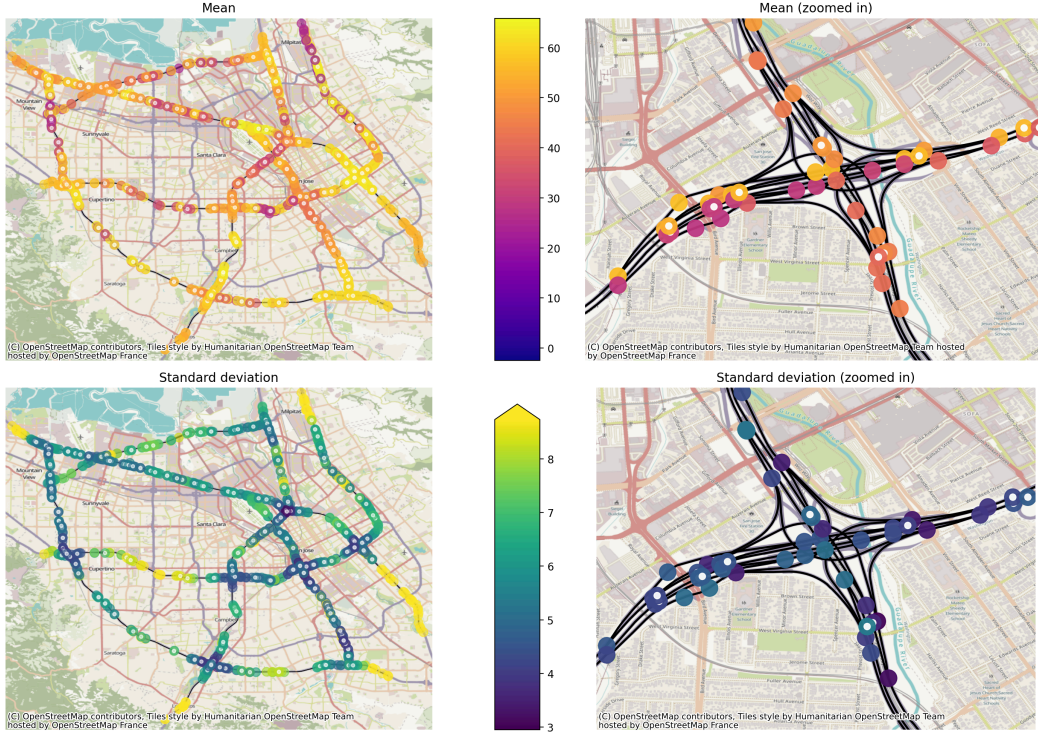


Figure 5: Posterior inference using GRF-GPs on the San Jose traffic network. **Top left:** Mean predictions across the full graph. **Top right:** Zoom-in shows directional differences between closely spaced lanes. **Bottom left:** Posterior uncertainty over the network. **Bottom right:** Zoomed view reveals local variation in confidence. Colored dots are sensor nodes; white dots indicate training nodes.

C.3 Large scale Bayesian optimisation on graphs

Bayesian optimisation on large graphs. We evaluated the scalability of GRF-GPs in Bayesian optimisation (BO) tasks on graphs with 10^6 nodes. The acquisition strategy is Thompson Sampling [30], [31], where samples are drawn from the posterior and maximisers are selected as evaluation points (shown in Alg. 3). We used pathwise conditioning for efficient posterior sampling.

Synthetic benchmarks. We consider four synthetic graph benchmarks:

- **Single-modal grid:** a 1000×1000 grid with a smooth central peak.
- **Periodic grid:** a 1000×1000 torus with smooth periodic variations.
- **Multi-modal grid:** a 1000×1000 grid with several randomly placed peaks.
- **Circular graph:** a ring of 10^6 nodes with sinusoidal variation.

All signals are perturbed with Gaussian noise ($\sigma_n^2 = 0.1$). Random features Φ are computed with 100 walks per node, with halting probability $p_{\text{halt}} = 0.1$. Walks longer than 5 hops are truncated.

Baselines. We compare GRFs-based Thompson Sampling against two search heuristics:

- **Random search:** uniformly samples nodes without replacement.
- **Breadth-first search (BFS):** greedily expands from the best observed node along adjacency structure.

BO setting: Each experiment was run for 50 BO iterations and repeated across 5 random seeds. At each iteration, we report *simple regret*, defined as the difference between the global maximum and the best function value observed so far.

Algorithm 3: Graph Thompson Sampling with GRFs

```
1 Inputs: black-box function  $f$ , candidate nodes  $\mathbf{x\_all}$ , initial sample size  $N_0$ , number of BO steps  $T$ .
2 Output: augmented dataset  $(\mathbf{x\_obs}, \mathbf{y\_obs})$ .
3 initialise  $\mathbf{x\_obs} \leftarrow \{x_i\}_{i=1}^{N_0}; x_i \sim \text{Unif}(\mathbf{x\_all})$ 
4 initialise  $\mathbf{y\_obs} \leftarrow \{f(x_i) + \varepsilon_i\}_{i=1}^{N_0}$ 
5 for  $t = 1, \dots, T$ 
6    $\text{model.train}(\mathbf{x\_obs}, \mathbf{y\_obs})$ 
7    $\mathbf{s\_t} \leftarrow \text{PosteriorSample}(\text{model}, \mathbf{x\_all})$ 
8    $\mathbf{x\_t} \leftarrow \text{ArgMax}(\mathbf{s\_t})$ 
9    $\mathbf{y\_t} \leftarrow f(\mathbf{x\_t}) + \varepsilon$ 
10   $\mathbf{x\_obs} \leftarrow \mathbf{x\_obs} \cup \mathbf{s\_t}$ 
11   $\mathbf{y\_obs} \leftarrow \mathbf{y\_obs} \cup \mathbf{y\_t}$ 
12 end for
13 return  $(\mathbf{x\_obs}, \mathbf{y\_obs})$ 
```

C.4 Classification task: Cora citation network

Here we provide more experimental details about the classification task on the Cora scientific citation network [32]. This experiment highlights the application of GRF-GPs in a more challenging, non-conjugate inference setting.

Dataset and preprocessing. The Cora dataset is a standard benchmark in graph-based machine learning. It consists of a citation network, where each node corresponds to a scientific publication and each edge represents a citation. Each publication is labeled with one of seven machine learning topics (Figure 6). While Cora also includes textual features, we focus solely on the graph structure.

Using a similar setup of Borovisky et al., we extract the largest connected component of the citation graph, resulting in a subgraph with 2,485 nodes and 5,069 edges.

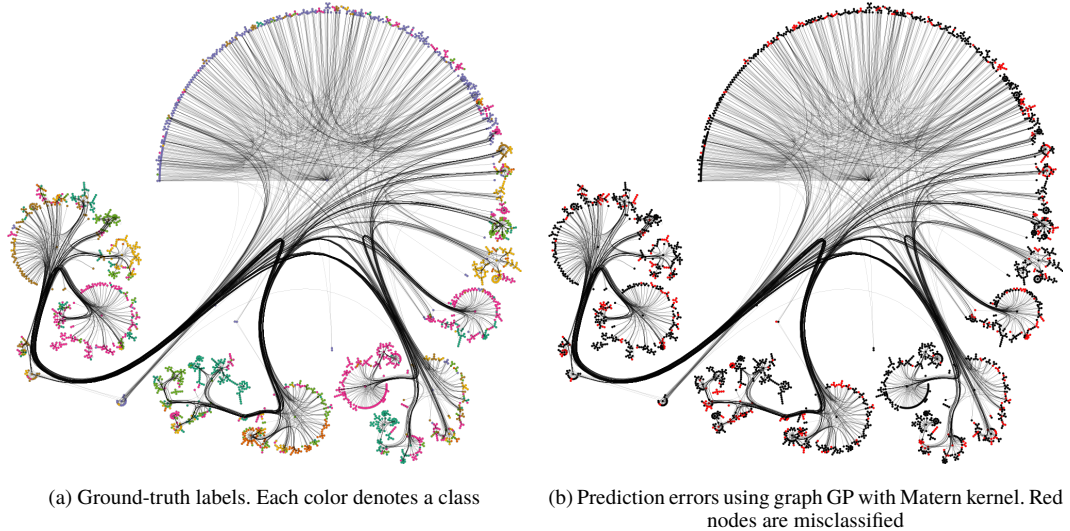


Figure 6: Cora dataset classification with graph GP.

Sparse variational inference for classification. Classification uses a non-Gaussian (softmax) likelihood, so the posterior is not analytically tractable. Denote the N_{train} training nodes as \mathbf{x} and \mathbf{z} the M inducing nodes. Define latent vectors $\mathbf{g} = (g(x) : x \in \mathbf{x})$ and $\mathbf{u} = (u(z) : z \in \mathbf{z})$. Assume a

GP prior $p(\mathbf{u}) = N(\mathbf{0}, \mathbf{K}_{uu})$ and a likelihood $p(y_i | g_i)$ (softmax). Choose a Gaussian variational posterior $q(\mathbf{u}) = N(\boldsymbol{\mu}, \boldsymbol{\Sigma})$ and induce the marginal $q(\mathbf{g}) = \int p(\mathbf{g} | \mathbf{u})q(\mathbf{u})d\mathbf{u}$. Under this approximation we optimize the evidence lower bound (ELBO):

$$\mathcal{L}_{\text{ELBO}} = \sum_{i=1}^{N_{\text{train}}} E_{q(g_i)}[\log p(y_i | g_i)] - \text{KL}(q(\mathbf{u}) \parallel p(\mathbf{u})).$$

This variational treatment replaces the intractable posterior with a tractable family and supplies a principled objective (a lower bound on $\log p(\mathbf{y})$); it yields coherent predictive distributions by integrating over $q(\mathbf{g})$ rather than relying on point approximations, which is especially important when the likelihood breaks conjugacy.

Training details. We use an 80/20 train-test split on the entire dataset. The goal is to predict the class labels of all nodes based on the graph structure alone. All models are trained using softmax likelihood. Optimization is performed for up to 1000 epochs using the Adam optimizer. To reduce uncertainty and assess variability, each configuration is repeated five times with different random seeds. The sparsity of the resulting GRFs kernels are also measured.